

# Accurate quantum-centric simulations of supramolecular interactions

Danil Kaliakin,<sup>1</sup> Akhil Shajan,<sup>1,2</sup> Javier Robledo Moreno,<sup>3</sup> Zhen Li,<sup>1</sup> Abhishek Mitra,<sup>1</sup> Mario Motta,<sup>3</sup> Caleb Johnson,<sup>3</sup> Abdullah Ash Saki,<sup>3</sup> Susanta Das,<sup>1</sup> Iskandar Sitdikov,<sup>3</sup> Antonio Mezzacapo,<sup>3</sup> and Kenneth M. Merz Jr.<sup>1,2,\*</sup>

<sup>1</sup>*Center for Computational Life Sciences,  
Lerner Research Institute, The Cleveland Clinic,  
Cleveland, Ohio 44106, United States*

<sup>2</sup>*Department of Chemistry, Michigan State University,  
East Lansing, Michigan 48824, United States*

<sup>3</sup>*IBM Quantum, IBM T.J. Watson Research Center,  
Yorktown Heights, NY 10598, United States*

We present the first quantum-centric simulations of noncovalent interactions using a supramolecular approach. We simulate the potential energy surfaces (PES) of the water and methane dimers, featuring hydrophilic and hydrophobic interactions, respectively, with a sample-based quantum diagonalization (SQD) approach. Our simulations on quantum processors, using 27- and 36-qubit circuits, are in remarkable agreement with classical methods, deviating from complete active space configuration interaction (CASCI) and coupled-cluster singles, doubles, and perturbative triples (CCSD(T)) within 1 kcal/mol in the equilibrium regions of the PES. Finally, we test the capacity limits of the quantum methods for capturing hydrophobic interactions with an experiment on 54 qubits. These results mark significant progress in the application of quantum computing to chemical problems, paving the way for more accurate modeling of noncovalent interactions in complex systems critical to the biological, chemical and pharmaceutical sciences.

---

\* [kmerz1@gmail.com](mailto:kmerz1@gmail.com)

## I. INTRODUCTION

The accurate treatment of noncovalent interactions [1, 2] is extremely important in the biological, chemical, and pharmaceutical sciences [3, 4]. Specifically, non-covalent interactions between hydrophobic species and hydrogen-bonded pairs play pivotal roles in a myriad of biological processes, ranging from protein folding [5–9] membrane assembly [10], cell signaling [11] and drug discovery [12–16]. The correct modeling of these interactions along with solvation plays a key role in understanding many chemical and biological processes [17].

Traditionally, quantum mechanical [18, 19] methods have been used to study these systems to a high level of accuracy - so-called chemical accuracy ( $\pm 1$  kcal/mol from experiment). However, these calculations are quite expensive and approaches to accelerate these calculations continue to be explored using classical hardware. [20–29] Using the results from these calculations, force fields have been fine-tuned for wide use in molecular simulation studies of chemical and biological processes [30–34]. More recently, machine learning [35] methods built using accurate quantum chemical calculations on thousands of systems have appeared to study largely covalent interactions, but can be extended to non-covalent interactions at a good level of accuracy, but at a reduced computational cost. However, these latter methods build models that can struggle to study diverse systems outside of the training set and can be subject to overfitting [36, 37].

Quantum computing based studies of these interactions, to a high level of accuracy and speed, would revolutionize our ability to understand complex processes like drug binding, but would also allow for the development of large synthetic datasets that could be used to build even better force fields and quantum machine learning models. However, to date, quantum hardware has struggled to address these problems. In this work we demonstrate that quantum-centric supercomputing (QCSC) [38] combined with the sample-based quantum diagonalization (SQD) approach [39] allows for the study of intermolecular interactions.

QCSC is a new computational paradigm, in which a quantum computer operates in concert with classical high-performance computing (HPC) resources. Classical processing carried out before, during, and after quantum computations allows for the introduction of quantum subroutines in the workflow of classical HPC algorithms, to extract and amplify signal from noisy quantum devices, and to leverage quantum processors to execute a limited

number of large quantum circuits.

The QCSC architecture enables scaling of computational capabilities, as exemplified by methods that use classical diagonalization in subspaces determined by quantum samples such as SQD [39] and QSCI [40]. The SQD method is developed based on QSCI. The SQD method use a quantum device to sample electronic configurations from a quantum circuit approximating the ground state of a molecular Hamiltonian, and use classical distributed HPC resources to post-process quantum measurements against known symmetries to obtain recovered configurations [39], as well as to solve the Schrödinger equation in the subspace spanned by the recovered configurations. The SQD method recently allowed us to address instances of the electronic structure problem with up to 36 spatial orbitals using up to 77 qubits [39]. The QCSC workflows produced significant improvements over simulations using quantum computers in isolation – which have in the last decade, used up to a handful of qubits with limited accuracies [41–78]. The QCSC paradigm coupled with SQD enables the study of problems heretofore out of reach of quantum computers including static correlation in iron-sulfur complexes [39] and well as dynamical correlation as exemplified in the intermolecular interactions studied herein.

Past studies have reported the simulation of noncovalent interactions [79, 80] using symmetry-adapted perturbation theory (SAPT). This method expresses the interaction energy through a perturbative treatment of the intermolecular potential [81–83], and requires the simulation of electronic structure of individual monomers on a quantum computer. In addition Anderson et al. demonstrated the possibility of simulations of coarse-grained intermolecular interactions on quantum computer as well. [84] However, to date, predicting binding energies between monomers using the supramolecular approach, where the electronic structure of entire dimer need to be simulated on quantum hardware, has been an elusive target for quantum simulations, due to lack of accuracy and scale of conventional quantum approaches.

Herein, we present the first quantum-centric simulation for the modeling of noncovalent hydrophilic and hydrophobic interactions with a supramolecular approach. We simulate the potential energy surfaces (PES) of the water dimer and the methane dimer. Our water dimer simulations use 27-qubit circuits, while the methane dimer simulations use 36- and 54-qubit circuits. To assess the accuracy of our quantum solutions, we compare them against heat-bath configuration interaction (HCI) [85–88] in the case of (16e,24o) calculations, complete

active space configuration interaction for the (16e,12o) and (16e,16o) calculations, as well as coupled-cluster singles, doubles and perturbative triples (CCSD(T)) [89] performed for all of the studied instances. The latter is widely recognized as the gold standard for computing intermolecular interactions [90] to chemical accuracy. For the 27-qubit water dimer and the 36-qubit methane dimer simulations, we demonstrate that SQD energies agree with CASCI nearly exactly, while deviating from CCSD(T) within 1 kcal/mol in the equilibrium region of the PES. For the 54-qubit simulations of the methane dimer, we observe how the accuracy of the quantum solution can be systematically improved by increasing the number of sampled configurations.

## II. METHODS AND COMPUTATIONAL DETAILS

### A. Classical benchmark

In the supramolecular approach binding energies between two monomers in a dimer is most often expressed as

$$E_{\text{binding}} = E_{AB} - E_A - E_B . \quad (1)$$

In Eq. (1)  $E_{AB}$ ,  $E_A$ , and  $E_B$  denote the ground-state energies of the dimer  $AB$ , monomer  $A$ , and monomer  $B$ , respectively. For calculations utilizing active spaces the highest accuracy obtainable with the supramolecular approach can be achieved if Eq. (1) is instead expressed in terms of the energy of bound and unbound dimers ( $E_{AB\text{-bound}}$  and  $E_{AB\text{-unbound}}$ ). Better accuracy is achieved within this approximation due to the fact that it allows for a consistent active space in all of the calculations. Hence, in all of our calculations we express the binding energy as

$$E_{\text{binding}} = E_{AB\text{-bound}} - E_{AB\text{-unbound}} . \quad (2)$$

Here, the  $E_{AB\text{-unbound}}$  term of Eq. (2) is approximated as two monomers separated by a 48.000 Å distance, where the chosen distance guarantees the absence of interactions between the monomers.

Metz et al [91] and Li et al. [92] demonstrated that CCSD(T)/aug-cc-pVQZ calculations closely reproduce the results of the CCSD(T)/complete basis set (CBS) limit for the methane dimer. Metz et al. [91] also demonstrated this for water dimer. All of our simulations are

Table I. Active spaces used in the present work.

species	active space AOs	Figure
water dimer	(16e,12o) O[2s,2p], H[1s]	1a
methane dimer	(16e,16o) C[2s,2p], H[1s]	1b
methane dimer	(16e,24o) C[2s,2p,3s,3p], H[1s,2s]	1c

therefore done with the aug-cc-pVQZ basis set. We simulate the water and methane dimers with the active spaces listed in Table I.

We construct these active spaces using the atomic valence active space (AVAS) method [93] as implemented in the PySCF 2.6.2 software package [94–96], and select active-space orbitals that overlap with the atomic orbitals (AOs) listed in column 3 of the table. The active-space orbitals of the water and methane dimers are shown in Fig. 1. Orbital visualization is performed with Pegamoid.[97]

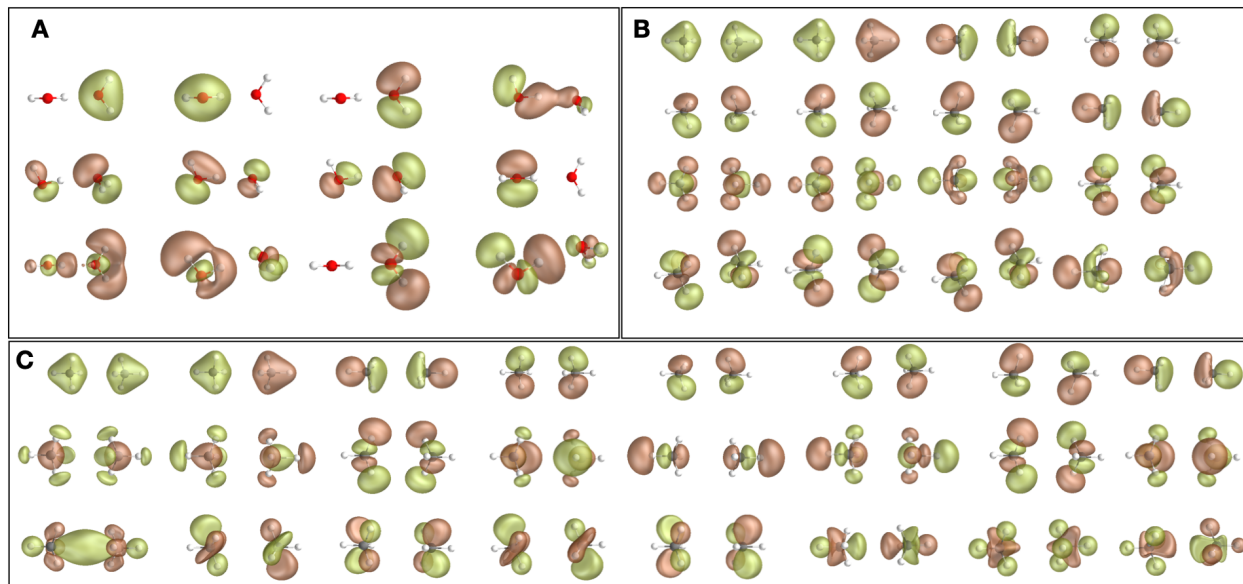


Figure 1. Active spaces used in this work: (A) (16e,12o) of the water dimer, (B) (16e,16o) of the methane dimer, (C) (16e,24o) of the methane dimer.

In each active space, we perform CCSD and CCSD(T) calculations with PySCF 2.6.2. For water and methane dimers we also perform CASCI(16e,12o) and CASCI(16e,16o) simulations, respectively, using PySCF 2.6.2. For the (16e,24o) active space of the methane dimer we perform HCI calculations with the SHCI-SCF 0.1 interface between PySCF 2.6.2

and DICE 1.0 [85, 87, 88]. Further details of HCI calculations can be found in the Supplementary Information. Along with active-space simulations, we perform complete CCSD and CCSD(T) calculations with ORCA 5.0.4 [98]. The geometries of equilibrium structures of the water and methane dimer originate from works by Temelso et al [99] and by Rezac and Hobza [100], sourced through the BEGDB database [101]. We describe the generation of PES geometries for water and methane dimers in the Supplementary Information.

## B. Quantum Computing

We start from the active-space Hamiltonian, written in second quantization as

$$\hat{H} = E_0 + \sum_{\substack{pr \\ \sigma}} h_{pr} \hat{a}_{p\sigma}^\dagger \hat{a}_{r\sigma} + \sum_{\substack{prqs \\ \sigma\tau}} \frac{(pr|qs)}{2} \hat{a}_{p\sigma}^\dagger \hat{a}_{q\tau}^\dagger \hat{a}_{s\tau} \hat{a}_{r\sigma}, \quad (3)$$

where  $\hat{a}^\dagger$  ( $\hat{a}$ ) are creation (annihilation) operators,  $p, r, s$ , and  $q = 1 \dots M$  denote basis set element,  $\sigma$  and  $\tau$  denote spin- $z$  polarizations,  $h_{pr}$  and  $(pr|qs)$  are the one- and two-body electronic integrals, and  $E_0$  is a constant accounting for the electrostatic interactions between nuclei and electrons in occupied inactive orbitals. We obtain the quantities  $E_0$ ,  $h_{pr}$ , and  $(pr|qs)$  for the selected active spaces using PySCF.

We prepare our wavefunction guesses  $|\Psi\rangle$ , used to approximate the ground state of Eq. (3), from a truncated version of the local unitary cluster Jastrow (LUCJ) ansatz [102]

$$|\Psi\rangle = \prod_{\mu=0}^{L-1} e^{\hat{K}_\mu} e^{i\hat{J}_\mu} e^{-\hat{K}_\mu} |\mathbf{x}_{\text{RHF}}\rangle, \quad (4)$$

where  $\hat{K}_\mu = \sum_{pr,\sigma} K_{pr}^\mu \hat{a}_{p\sigma}^\dagger \hat{a}_{r\sigma}$  are one-body operators,  $\hat{J}_\mu = \sum_{pr,\sigma\tau} J_{p\sigma,r\tau}^\mu \hat{n}_{p\sigma} \hat{n}_{r\tau}$  are suitable (vide infra) density-density operators, and  $|\mathbf{x}_{\text{RHF}}\rangle$  is the restricted closed-shell Hartree-Fock (RHF) state. We use the Jordan-Wigner (JW) transformation [103] to map the fermionic wavefunction Eq. (4) onto a qubit wavefunction that can be prepared executing a quantum circuit. The JW transformation maps the Fock space of fermions in  $M$  spatial orbitals onto the Hilbert space of  $2M$  qubits, where the basis state  $|\mathbf{x}\rangle$  is parametrized by a bitstring  $\mathbf{x} \in \{0, 1\}^{2M}$  and represents an electronic configuration where the spin-orbital  $p\sigma$  is occupied (empty) if  $x_{p\sigma} = 1$  ( $x_{p\sigma} = 0$ ). We prepare the wavefunction Eq. (4) by executing the following quantum circuit: a single layer of Pauli-X gates prepares the basis state  $|\mathbf{x}_{\text{RHF}}\rangle$ , a Bogoliubov circuit [104] (with linear depth, quadratic number of gates, and a 1D qubit

connectivity) encodes each orbital rotation  $e^{\pm\hat{K}_\mu}$ , and a circuit of Pauli-ZZ rotations encodes each density-density interaction  $e^{i\hat{J}_\mu}$ . When  $J^\mu$  is a dense matrix, Pauli-ZZ rotations are applied across all pair of qubits, requiring all-to-all qubit connectivity or a substantial overhead of swap gates. To mitigate these quantum hardware requirements LUCJ imposes a “locality” approximation, i.e., it assumes  $J_{\rho\sigma,r\tau}^\mu = 0$  for all pairs of spin-orbitals that are not mapped onto adjacent qubits under JW [102] (as a consequence, a circuit with constant depth and linear number of gates encodes each  $e^{i\hat{J}_\mu}$  operator). Hence, the number of layers ( $L - 1$ ) in Eq. (4) is formally equal to 1.5. As the result the specific form of  $|\Psi\rangle$  used in this work is expressed as  $|\Psi\rangle = e^{-\hat{K}_2} e^{\hat{K}_1} e^{i\hat{J}_1} e^{-\hat{K}_1} |\mathbf{x}_{\text{RHF}}\rangle$ . We parametrize the LUCJ circuit based on amplitudes computed from classical restricted closed-shell CCSD within the given active space [39], yet a further quantum-classical parameter optimization could further improve the quality of the ground-state approximation. We produce the LUCJ circuits using the ffsim library [105] interfaced with Qiskit 1.1.1 [104, 106].

The qubit layouts of the LUCJ circuits used for (16e,12o) water dimer, (16e,16o) methane dimer, and (16e,24o) methane dimer simulations are shown in Fig. 2a, 2b, and 2c, respectively. We execute these circuits on IBM’s 127-qubit Eagle devices `ibm_cleveland` and `ibm_kyiv`. In all our quantum computing experiments, we used gate (not measurement) twirling over random 2-qubit Clifford gates [107] and dynamical decoupling [108–111] – available through the `SamplerV2` primitive of Qiskit’s runtime library – to mitigate quantum errors.

Upon executing the LUCJ circuits, we measure  $|\Psi\rangle$  in the computational basis. Repeating this produces a set of measurement outcomes (or “shots”)

$$\tilde{\chi} = \{\mathbf{x} | \mathbf{x} \sim \tilde{p}(\mathbf{x})\} \quad (5)$$

in the form of bitstrings  $\mathbf{x} \in \{0, 1\}^{2M}$ , each representing an electronic configuration (Slater determinants) distributed according to  $\tilde{p}(\mathbf{x})$ . While on a noiseless device configurations are distributed according to  $|\langle \mathbf{x} | \Psi \rangle|^2$ , on a noisy device they follow a distribution  $\tilde{p}(\mathbf{x}) \neq |\langle \mathbf{x} | \Psi \rangle|^2$ . In particular,  $\tilde{p}(\mathbf{x})$  breaks particle-number conservation and returns configurations with incorrect particle number. We use a technique called self-consistent configuration recovery [39], executed on a classical computer, to restore particle-number conservation. The associated code is publicly available in the GitHub repository. [112] Within each step of self-consistent recovery, we sample  $K$  subsets (or batches) of  $\tilde{\chi}$  labeled  $\tilde{\chi}_b$  with  $b = 1 \dots K$ .

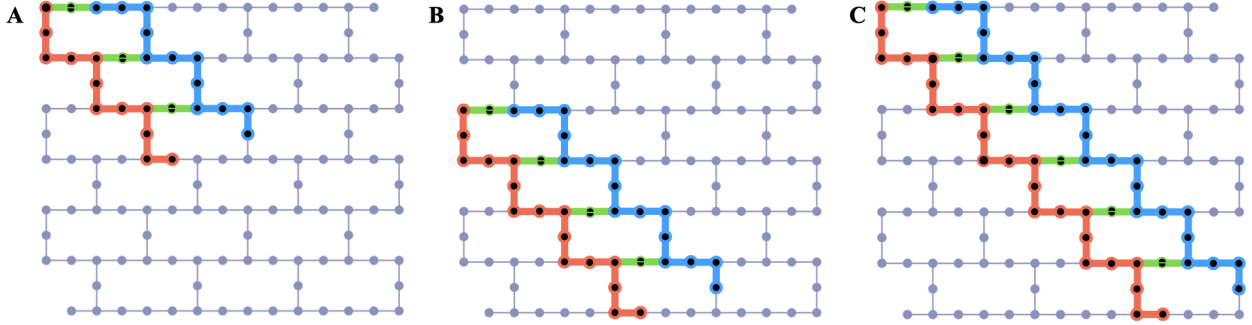


Figure 2. Qubit layouts of LUCJ circuits executed in this work: (A) (16e,12o) water dimer simulations using 27 qubits on `ibm_cleveland`, (B) (16e,16o) methane dimer simulations using 36 qubits on `ibm_cleveland`, and (C) (16e,24o) methane dimer simulations using 54 qubits on `ibm_kyiv`. Qubits used to encode occupation numbers of  $\alpha$  ( $\beta$ ) spin-orbitals are shown in red (blue). Auxiliary qubits used to execute density-density interactions between  $\alpha$  and  $\beta$  spin-orbitals are marked in green.

Each batch defines – through a transformation [39] informed by an approximation to the ground-state occupation numbers  $n_{p\sigma}$  – a subspace  $S^{(b)}$  of dimension  $d$ , in which we project the many-electron Hamiltonian as [39, 40, 113]

$$\hat{H}_{S^{(b)}} = \hat{P}_{S^{(b)}} \hat{H} \hat{P}_{S^{(b)}} , \quad (6)$$

where the projector  $\hat{P}_{S^{(b)}}$  is

$$\hat{P}_{S^{(b)}} = \sum_{\mathbf{x} \in S^{(b)}} |\mathbf{x}\rangle \langle \mathbf{x}| . \quad (7)$$

We compute the ground states and energies of the Hamiltonians in Eq. (6),  $|\psi^{(b)}\rangle$  and  $E^{(b)}$  respectively, and use the lowest energy across the batches,  $\min_b E^{(b)}$ , as the best approximation to the ground-state energy at the current iteration of the configuration recovery. We use the ground states  $|\psi^{(b)}\rangle$  to obtain an updated set of occupation numbers,

$$n_{p\sigma} = \frac{1}{K} \sum_{1 \leq b \leq K} \langle \psi^{(b)} | \hat{n}_{p\sigma} | \psi^{(b)} \rangle , \quad (8)$$

that we use in the next iteration of configuration recovery to produce the subspaces  $S^{(b)}$ . We repeat the iterations of self-consistent configuration recovery until convergence of the energy  $\min_b E^{(b)}$ . At the first iteration of self-consistent configuration recovery, we initialize  $n_{p\sigma}$  from the measurement outcomes in  $\tilde{\chi}$  with the correct particle number. We summarize the details of our SQD calculations in Table II.



Table II. Details of SQD calculations.

species	active space	$ \tilde{\chi}  [10^3]$	$K$	$ \tilde{\chi}_b  [10^3]$	$d$	CPU, code	steps
water dimer	(16e,12o)	200	10	10	$24.5 \cdot 10^4$	10, PySCF	10
methane dimer	(16e,16o)	200	10	20	$12.6 \cdot 10^7$	10, PySCF	10
methane dimer	(16e,24o)	300	4	8.5	$24.9 \cdot 10^7$	20, DICE	5

We demonstrate that for SQD (16e,16o) simulations of the methane dimer at 3.638 Å a  $|\tilde{\chi}_b| = 20.0 \cdot 10^3$  is necessary to reach agreement within 0.010 kcal/mol when compared against CASCI (16e,16o). We show how the predicted total energies in these simulations improve with an increase of  $|\tilde{\chi}_b|$  from  $5.0 \cdot 10^3$  to  $20.0 \cdot 10^3$  in Figure S3. We also demonstrate that in SQD(16e,16o) simulations the linear energy-variance relation allows for utilization of energy extrapolation which reproduces similar binding energies as simulation with  $|\tilde{\chi}_b| = 20.0 \cdot 10^3$  while using substantially lower values of  $|\tilde{\chi}_b|$ . The extrapolation is done for the total energy of the dimer as the function of the Hamiltonian variance divided by the square of the variational energy, where Hamiltonian variance ( $\Delta H$ ) is calculated as  $\Delta H = \langle \psi^{(k)} | \hat{H}^2 | \psi^{(k)} \rangle - \langle \psi^{(k)} | \hat{H} | \psi^{(k)} \rangle^2$ . The extrapolation is done based on three points with  $|\tilde{\chi}_b|$  of  $9.0 \cdot 10^3$ ,  $11.0 \cdot 10^3$ , and  $14.0 \cdot 10^3$ , which allows for the reduction of the maximum  $|\tilde{\chi}_b|$  by  $6.0 \cdot 10^3$ . This choice of values for  $|\tilde{\chi}_b|$  allows for an even distribution of  $\Delta H$  values used in extrapolation. The extrapolated energies are compared against CASCI(16e,16o) simulations and SQD(16e,16o) simulations with  $|\tilde{\chi}_b| = 20.0 \cdot 10^3$ .

We compute the ground-state eigenpairs of the Hamiltonians Eq. (6) using the iterative Davidson method on 10 CPUs with PySCF’s selected configuration interaction (SCI) solver for SQD (16e,12o) simulations of the water dimer and SQD (16e,16o) simulations of the methane dimer. We achieve parallelization across 10 CPUs with Ray 2.33.0 [114] where the eigenstate solver within each of the 10 batches is using 1 CPU. For SQD (16e,24o) simulations of the methane dimer, we utilize the SCI solver of DICE and 20 CPUs, where the eigenstate solver within each of the 5 batches is using 4 CPUs. Further parallelization is possible with the SCI solver of DICE, as was demonstrated previously [39]. The SQD (16e,12o) simulations of the water dimer and SQD (16e,16o) simulations of the methane dimer are done for the distances that are described in the Supplemental Information while SQD (16e,24o) simulations of the methane dimer are only done for 3.638 Å.

### III. RESULTS

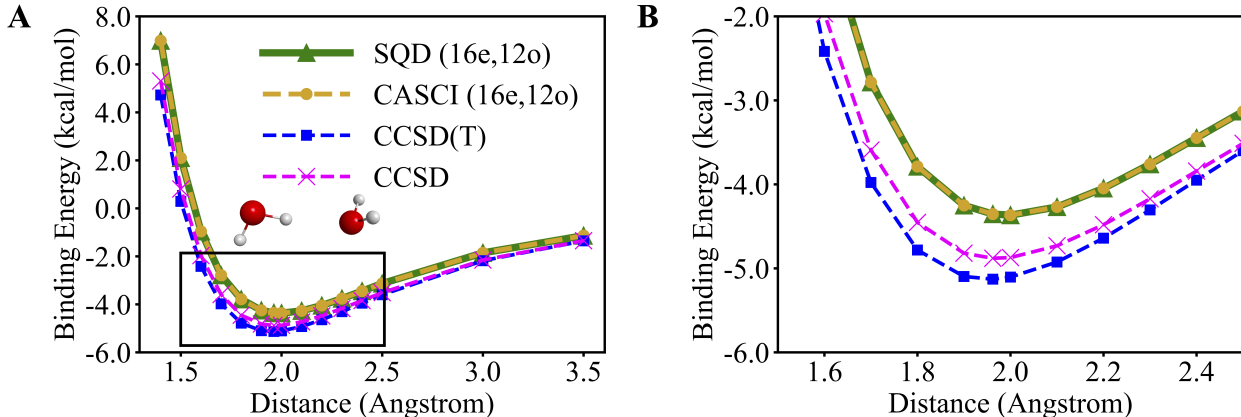


Figure 3. Binding energies of the water dimer along the PES, where distances between oxygen atoms range between 1.400 and 3.500 Å. (A) the entire range of bondlengths, and (B) a magnified region near equilibrium, highlighted in panel (A) as a black box. Light brown, blue, and magenta dashed lines with circle, square, and cross markers depict the PES calculated with the CASCI (16e,12o), CCSD(T), and CCSD methods, respectively. The solid green line with triangular markers depicts the PES calculated with the SQD (16e,12o).

Figure 3 shows the binding energy of the water dimer as a function of the oxygen-oxygen distance using SQD and CASCI. The SQD and CASCI potential energy surfaces closely align, deviating from each by less than 0.001 kcal/mol. This close alignment is an indication that both methods have accurately solved the Schrodinger equation in the active space. The active-space SQD and CASCI calculations cannot capture dynamical correlation from inactive orbitals. To quantify the extent of the active-space approximation, we also compute the potential energy surface using CCSD and CCSD(T) in the full aug-cc-pVQZ basis. The perturbative triples do not have a drastic effect on the binding energy between water monomers and the close agreement between CCSD and CCSD(T) calculations is shown in Figure 3b. The excellent agreement between CCSD and CCSD(T) in the full basis and between SQD and CASCI in the active space indicates that the differences between SQD and CCSD(T) are due to the active-space approximation underlying the former. The CCSD(T) and SQD potential energy curves are in reasonable agreement with each other, the highest deviation being observed at 1.400 Å and corresponding to 2.263 kcal/mol. Despite this reasonable agreement and the ability of SQD to capture hydrogen bonding, there are quan-

titative differences in the predicted binding energies,  $-5.129$  kcal/mol and  $-4.366$  kcal/mol for CCSD(T) and SQD respectively, and the lowest-energy distances,  $1.962$  Å and  $2.000$  Å for CCSD(T) and SQD respectively. The quantitative differences between SQD and CCSD and CCSD(T) shown in Fig. 3 are a consequence of SQD not being carried out in the full basis set.

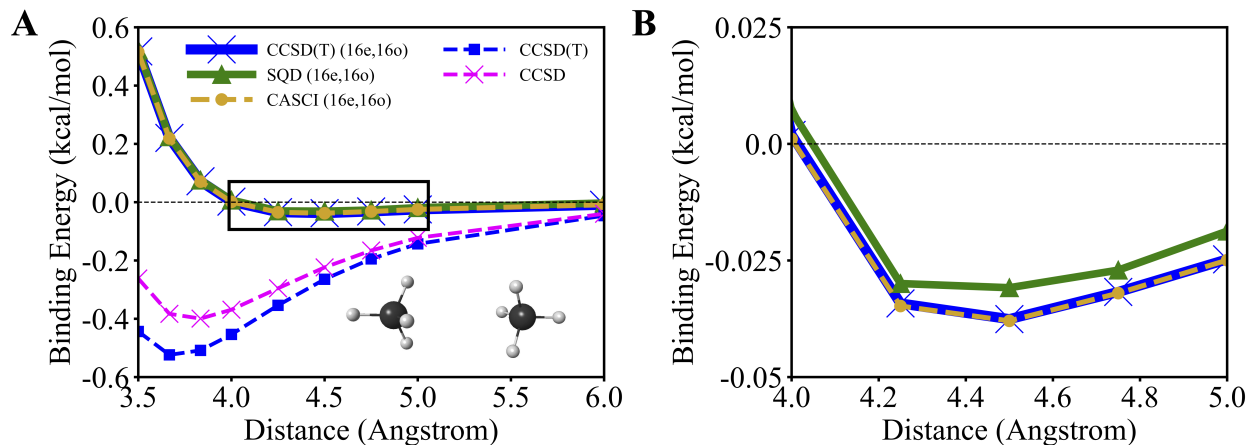


Figure 4. Binding energies of the methane dimer along the PES, where the distances between the carbon atoms range between  $3.500$  and  $6.000$  Å. Active-space simulations use (16e,16o). (A) the entire range of bondlengths, and (B) a magnified region near equilibrium, highlighted in panel (A) as a black box. Light brown, blue, and magenta dashed lines with circle, square, and cross markers depict the PES calculated with the CASCI (16e,16o), CCSD(T), and CCSD methods, respectively. The solid green line with triangular markers depicts the PES calculated with the SQD (16e,16o). The solid blue line represents CCSD(T) (16e,16o) calculations. The black horizontal dashed line indicates the zero value of the binding energy.

Figure 4 shows the binding energy of the methane dimer – with (16e,16o) active space for the dimer and monomer respectively – as a function of the carbon-carbon distance using SQD and HCI. Figure 4 focuses on the attractive region, whereas the full curve is shown in Figure S5 of the SI. The SQD (16e,16o) and CASCI (16e,16o) data are closely aligned, with deviations below  $0.005$  kcal/mol. We interpret the excellent agreement between SQD (16e,16o) and CASCI (16e,16o) as an indication that the active-space Schrodinger equation is solved accurately. SQD (16e,16o) predicts the interaction between the monomers to be only marginally attractive, with a binding energy of  $-0.038$  kcal/mol and a lowest-energy distance around  $4.500$  Å. On the other hand, full-basis CCSD and CCSD(T) calculations

predict binding energies of -0.399 kcal/mol and -0.524 kcal/mol, respectively, at distances 3.834 Å and 3.667 Å, respectively. Despite some differences quantifying the importance of perturbative triple corrections, both full-basis calculations predict a substantially more pronounced tendency to binding than SQD (16e,16o) and CASCI (16e,16o). This is because, although SQD (16e,16o) and CASCI (16e,16o) calculations can accurately capture the active-space electronic correlation, they cannot account for the residual dynamical electron correlation, unlike full-basis CCSD and CCSD(T).

Before proceeding with the expansion of the active space we first demonstrate that accurate SQD (16e,16o) calculations can be achieved with a reduced number of samples through the extrapolation of the total energies. The exact SQD (16e,16o) calculations require  $|\tilde{\chi}_b| = 20.0 \cdot 10^3$  while the extrapolation is done based on three points with  $|\tilde{\chi}_b|$  of  $9.0 \cdot 10^3$ ,  $11.0 \cdot 10^3$ , and  $14.0 \cdot 10^3$ . Hence, the extrapolation allows for the reduction of the maximum required  $|\tilde{\chi}_b|$  by  $6.0 \cdot 10^3$ . We show the SQD (16e,16o) total energy extrapolations for 4.000, 4.250, 4.500, 4.750, 5.000, and 6.000 Å distances in Figure 5a-f, while the extrapolation for the 48.000 Å distance is shown in Figure 5g. The resulting binding energies of the methane dimer are shown in Figure 5h and compared against the CASCI (16e,16o) simulations and SQD (16e,16o) simulations with  $|\tilde{\chi}_b| = 20.0 \cdot 10^3$ . Figure 5g shows that the extrapolated SQD (16e,16o) energies predict a binding energy in good qualitative agreement with exact SQD (16e,16o) simulations and CASCI (16e,16o). This result is promising for future simulations with large active spaces, where classical post-processing of SQD data becomes computationally expensive.

Next we analyze the effect of extending the active space on the predicted binding energy via the inclusion of virtual orbitals with carbon 3s and 3p character. First, in Fig. 6, we explore the performance of HCI in this extended (16e,24o) active space. Here, HCI is used in place of CASCI due to the fact that the (16e,24o) active space is prohibitively expensive in conventional CASCI simulations. Figure 6a shows active-space calculations with HCI, CCSD, and CCSD(T). The CCSD(T) (16e,24o) curve, in good agreement with CCSD (16e,24o), is substantially more attractive than in the (16e,16o) active space, predicting a binding energy of -0.136 kcal/mol at 4.000 Å. The size of the (16e,24o) active space prevents us from significantly lowering the parameter  $\varepsilon_1$  which results in the underestimation of the total energy in HCI (16e,24o) calculations. In particular, at 3.834 Å distance the HCI (16e,24o) calculations underestimate the binding energy by 0.094 kcal/mol comparing to

CCSD(T) (16e,24o), as visible in Fig. 6b. Note that HCI (16e,24o) calculations were carried out over four distances (3.667, 3.750, 3.834, and 3.900 Å). Within the target accuracy of the

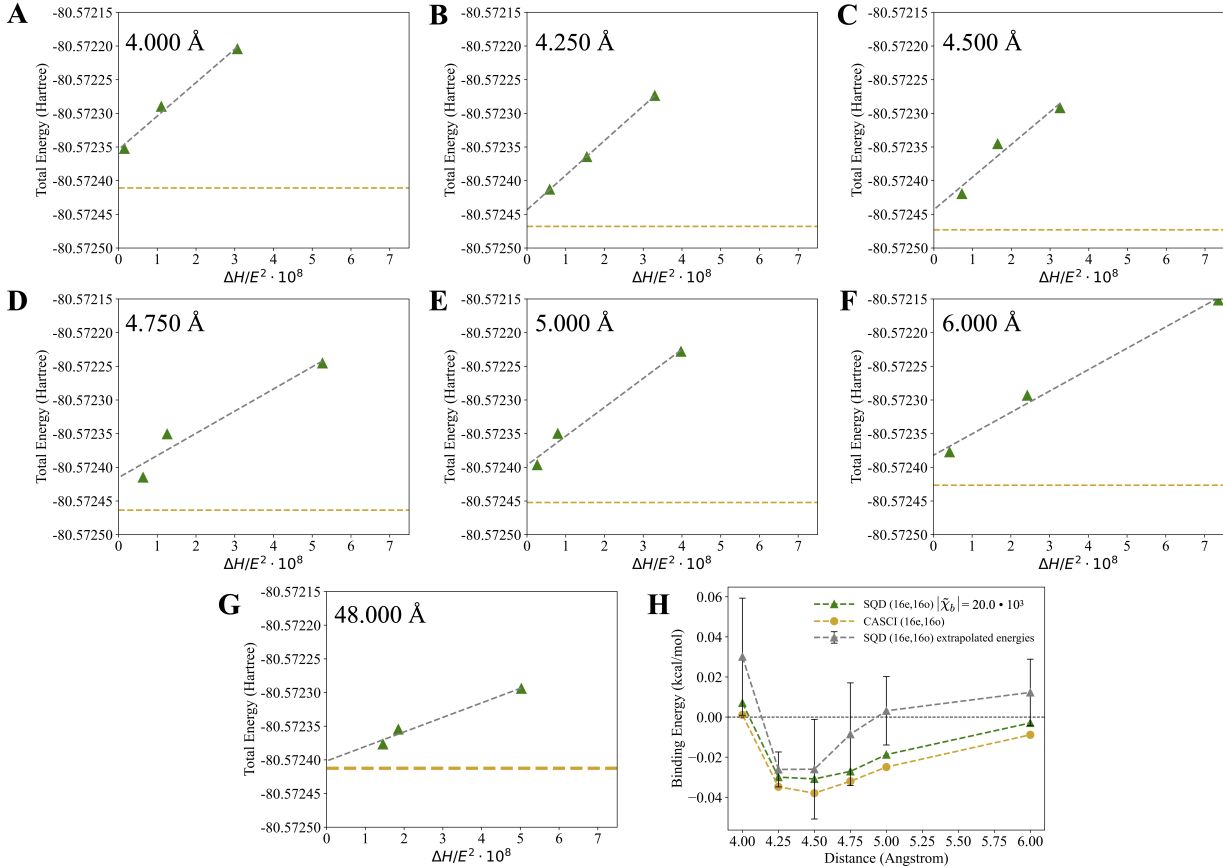


Figure 5. Extrapolated SQD (16e,16o) energies of the methane dimer along the PES, for the 4.000, 4.250, 4.500, 4.750, 5.000, and 6.000 Å distances between the carbon atoms. Extrapolations are done using three points with  $|\tilde{\chi}_b|$  of  $9.0 \cdot 10^3$ ,  $11.0 \cdot 10^3$ , and  $14.0 \cdot 10^3$ . Hamiltonian variance ( $\Delta H$ ) is calculated as  $\Delta H = \langle \psi^{(k)} | \hat{H}^2 | \psi^{(k)} \rangle - \langle \psi^{(k)} | \hat{H} | \psi^{(k)} \rangle^2$ . (A) - (F) total energy extrapolations for methane dimer 4.000, 4.250, 4.500, 4.750, 5.000, and 6.000 Å distances, (G) total energy extrapolations at 48.000 Å distance, and (H) binding energy in methane dimer calculated with extrapolated SQD (16e,16o) total energies compared against CASCI (16e,16o) simulations and SQD (16e,16o) simulations with  $|\tilde{\chi}_b| = 20.0 \cdot 10^3$ . Green triangles and green dashed lines indicate SQD (16e,16o) energies calculated with  $|\tilde{\chi}_b| = 20.0 \cdot 10^3$ . Grey triangles and grey dashed lines indicate extrapolated SQD (16e,16o) energies. Light brown circles and dashed lines indicate CASCI (16e,16o) energies. Black horizontal dashed line indicates the zero value of the binding energy. Error bars indicate magnitude of error estimate in extrapolation.

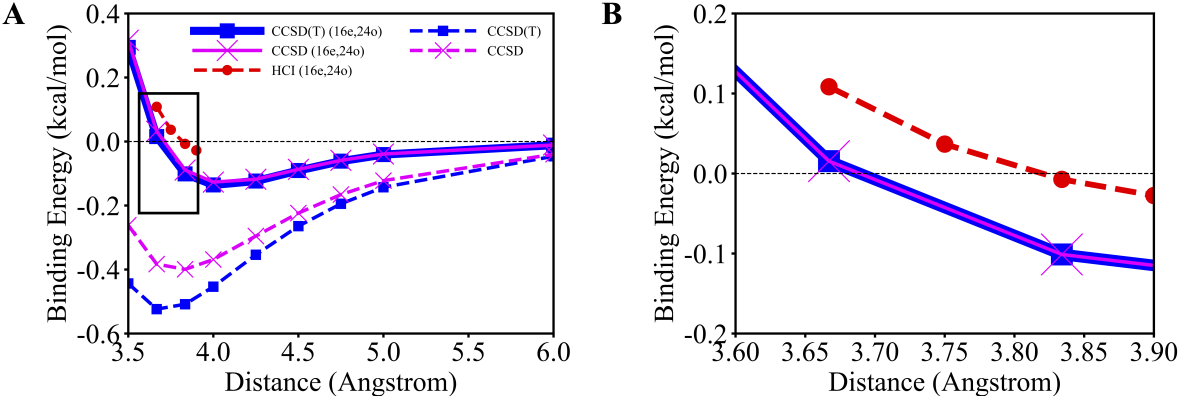


Figure 6. Binding energies of the methane dimer along the PES, where the distances between the carbon atoms range between 3.500 and 6.000 Å. Active-space simulations use (16e,24o) and are performed over (A) the entire range of bondlengths, and (B) a magnified region near equilibrium, highlighted in panel (A) as a black box. Blue and magenta dashed lines depict PES calculated with CCSD(T) and CCSD methods, respectively. The dashed red line depicts the HCI (16e,24o) results. The solid blue and magenta lines represents CCSD(T) (16e,24o) and CCSD (16e,24o) calculations, respectively. Black horizontal dashed line indicates the zero value of the binding energy.

present work the prediction of HCI (16e,24o) binding energies for other geometries around the CCSD(T) (16e,24o) minimum is dramatically more computationally expensive.

We show the decrease in the SQD (16e,24o) total energy for the methane dimer at 3.638 Å with the increase of  $|\tilde{\chi}_b|$  from  $5.0 \cdot 10^3$  to  $8.5 \cdot 10^3$  in Fig. 7. The differences between the total energies predicted with SQD (16e,24o) and HCI (16e,24o) reduce from 31.8 milliHartree to 25.2 milliHartree when the  $|\tilde{\chi}_s|$  is increased from  $5.0 \cdot 10^3$  to  $8.5 \cdot 10^3$ . The extrapolated total energy based on SQD (16e,24o) simulations with  $|\tilde{\chi}_b|$  of  $5.5 \cdot 10^3$ ,  $6.5 \cdot 10^3$ ,  $7.5 \cdot 10^3$ , and  $8.5 \cdot 10^3$  agrees with HCI (16e,24o) results within 2.12 milliHartree. Magnitude of the error estimate in extrapolation is  $\pm 3.10$  milliHartree. We believe that a further increase in the number of samples will allow us to advance the accuracy of SQD (16e,24o) calculations. To make SQD (16e,24o) calculations of the methane dimer more computationally feasible we are currently exploring parallelization options for calculations on this system as well as the analysis of the configurations with low contributions to the total energies.

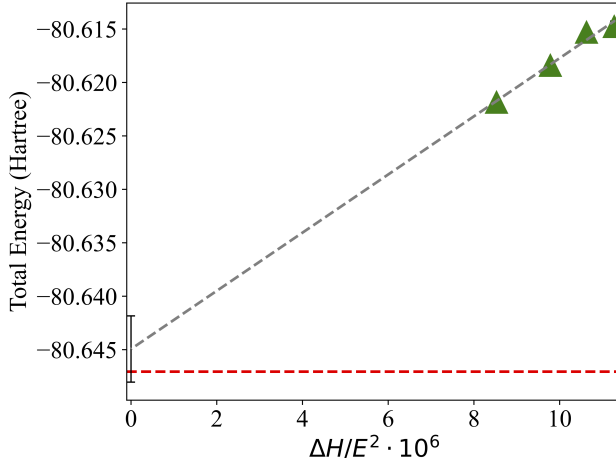


Figure 7. Extrapolation of SQD (16e,24o) total energies for the methane dimer at 3.638 Å distance between the carbon atoms. Extrapolations are done using four points with  $|\tilde{\chi}_b|$  of  $5.5 \cdot 10^3$ ,  $6.5 \cdot 10^3$ ,  $7.5 \cdot 10^3$ , and  $8.5 \cdot 10^3$ . Hamiltonian variance ( $\Delta H$ ) is calculated as  $\Delta H = \langle \psi^{(k)} | \hat{H}^2 | \psi^{(k)} \rangle - \langle \psi^{(k)} | \hat{H} | \psi^{(k)} \rangle^2$ . Green triangles indicate SQD (16e,24o) energies. Grey dashed lines indicate extrapolated SQD (16e,24o) energies. Dashed red line indicates HCI (16e,24o) energies. Error bars indicate magnitude of error estimate in extrapolation.

#### IV. CONCLUSIONS AND OUTLOOK

We have presented quantum-centric simulations of the water and methane dimers using a sample-based quantum diagonalization method on IBM’s Eagle quantum processors. This demonstration is a first simulation of noncovalent supramolecular interactions on quantum processors. The accuracy of SQD and HCI predictions of noncovalent interactions can be systematically improved by the addition of extended shells of virtual orbitals. We anticipate that further expansion of the active space through the inclusion of the virtual orbitals corresponding to the 3d shell of the heavy atoms will allow for an even more accurate description of non-covalent interactions with SQD and HCI, which will be the subject of future studies on quantum processors. Importantly, the present study lays out a framework for electronic structure calculations of noncovalent interactions on quantum hardware.

Our findings demonstrate that SQD is capable of capturing noncovalent interactions between molecules at the level of theory chosen, with potential energy surfaces that closely align with those obtained through classical computational methods. We examine the binding energies of the water and methane dimers by comparing SQD with an analogous classical

method, namely HCI. We also compare SQD against the CCSD(T) method, which is considered the gold standard for calculations of binding energies [90]. This comparison aims to evaluate the accuracy of SQD and to understand how the nature of the PES changes with different active-space selections. The ability of HCI and SQD to recover the dispersion interaction is highly dependent on the size and nature of the active space, which is especially critical for predicting the binding energy of the methane dimer. In fact, a previous study by Hapka et al.[115] demonstrated that the ability of supramolecular multiconfigurational interaction calculations to recover the dispersion energy depends on the size of the active space and can be improved with systematic expansion of the active space.

The results obtained here demonstrate the improvements both in terms of accuracy and scale of quantum computations on chemical problems, enabling, on current quantum processors, use cases previously thought to belong to the fault-tolerant domain, such as the largest active space considered here for methane, which has 1.3M Pauli operators. Further examples of problems that could be enabled by our approach include quantum computing simulations of chemical reactivity of  $CO_2$ -fixating ruthenium catalyst proposed by Burg et al. [116], Ibrutinib drug simulations proposed by Blunt et al.[117], and the drug-discovery workflows proposed by Pyrkov et al.[118] and Kumar et al.[119], as well as multiple stages of drug optimization as described by Bonde et al.[120] The SQD method allows for simulations of systems with qubit counts that is essential for projection-based embedding algorithm proposed by Ralli et al.[121] and can enhance the viability of fragment-based quantum computing simulations. Previously, VQE-based fragment molecular orbital (FMO),[122] divide and conquer (DC),[123] and density matrix embedding theory (DMET)[65, 124] simulations were limited to very simple illustrative systems. Shang et al. proposed a DMET-based massively parallel quantum computing approach based on VQE, but execution of their methodology was only possible on a quantum simulator rather than actual hardware.[125]

Such limitations in fragment-based VQE simulations are due to the fact that the number of orbitals that could be described with reasonable accuracy on actual hardware in the VQE formalism within each fragment is very limited. Fragment-based simulations with SQD would allow for substantially higher number of orbitals in each individual fragment, making the quantum computing simulations of proteins and drug molecules possible.

In conclusion, combining quantum and classical computational resources in workflows like SQD opens the way for the use of current and near-future quantum technology to tackle



computational challenges in small-molecule conformational search, drug-protein interactions and drug discovery.

## ACKNOWLEDGMENTS

The authors gratefully acknowledge financial support from the National Science Foundation (NSF) through CSSI Frameworks Grant OAC-2209717 and from the National Institutes of Health (Grant Numbers GM130641).

- 
- [1] K. Müller-Dethlefs and P. Hobza, Noncovalent interactions: a challenge for experiment and theory, *Chemical Reviews* **100**, 143 (2000).
  - [2] C. Puzzarini, L. Spada, S. Alessandrini, and V. Barone, The challenge of non-covalent interactions: Theory meets experiment for reconciling accuracy and interpretation, *Journal of Physics: Condensed Matter* **32**, 343002 (2020).
  - [3] W. J. Pichler, The important role of non-covalent drug-protein interactions in drug hypersensitivity reactions, *Allergy* **77**, 404 (2022).
  - [4] A. Aljoundi, I. Bjjj, A. El Rashedy, and M. E. Soliman, Covalent versus non-covalent enzyme inhibition: which route should we take? a justification of the good and bad from molecular modelling perspective, *The Protein Journal* **39**, 97 (2020).
  - [5] H. J. Dyson, P. E. Wright, and H. A. Scheraga, The role of hydrophobic interactions in initiation and propagation of protein folding, *Proceedings of the National Academy of Sciences* **103**, 13057 (2006), <https://www.pnas.org/doi/pdf/10.1073/pnas.0605504103>.
  - [6] N. J. Zondlo, Fold globally, bond locally, *Nature Chemical Biology* **6**, 567 (2010).
  - [7] C. N. Pace, H. Fu, K. L. Fryar, J. Landua, S. R. Trevino, B. A. Shirley, M. M. Hendricks, S. Imura, K. Gajiwala, J. M. Scholtz, and G. R. Grimsley, Contribution of hydrophobic interactions to protein stability, *J Mol Biol* **408**, 514 (2011).
  - [8] C. Camilloni, D. Bonetti, A. Morrone, R. Giri, C. M. Dobson, M. Brunori, S. Gianni, and M. Vendruscolo, Towards a structural biology of the hydrophobic effect in protein folding, *Scientific Reports* **6**, 28285 (2016).

- [9] S. R. Durell and A. Ben-Naim, Hydrophobic-hydrophilic forces in protein folding, *Biopolymers* **107**, [10.1002/bip.23020](https://doi.org/10.1002/bip.23020) (2017).
- [10] R. G. Hanshaw, R. V. Stahelin, and B. D. Smith, Noncovalent keystone interactions controlling biomembrane structure, *Chemistry* **14**, 1690 (2008).
- [11] V. A. Adhav and K. Saikrishnan, The realm of unconventional noncovalent interactions in proteins: Their significance in structure and function, *ACS Omega* **8**, 22268 (2023).
- [12] H. Jhoti and A. R. Leach, *Structure-Based Drug Discovery* (Springer Netherlands, 2007).
- [13] E. Gros, S. Deshayes, M. C. Morris, G. Aldrian-Herrada, J. Depollier, F. Heitz, and G. Divita, A non-covalent peptide-based strategy for protein and peptide nucleic acid transduction, *Biochimica et Biophysica Acta (BBA) - Biomembranes* **1758**, 384 (2006).
- [14] Y. Wei, L. Ma, L. Zhang, and X. Xu, Noncovalent interaction-assisted drug delivery system with highly efficient uptake and release of paclitaxel for anticancer therapy, *Int J Nanomedicine* **12**, 7039 (2017).
- [15] Y. Yang, H. Zhang, Y. Wanyan, K. Liu, T. Lv, M. Li, and Y. Chen, Effect of hydrophobicity on the anticancer activity of fatty-acyl-conjugated cm4 in breast cancer cells, *ACS Omega* **5**, 21513 (2020).
- [16] K. M. Wright, S. R. DiNapoli, M. S. Miller, P. Aitana Azurmendi, X. Zhao, Z. Yu, M. Chakrabarti, W. Shi, J. Douglass, M. S. Hwang, E. H. Hsiue, B. J. Mog, A. H. Pearlman, S. Paul, M. F. Konig, D. M. Pardoll, C. Bettgowda, N. Papadopoulos, K. W. Kinzler, B. Vogelstein, S. Zhou, and S. B. Gabelli, Hydrophobic interactions dominate the recognition of a kras g12v neoantigen, *Nat Commun* **14**, 5063 (2023).
- [17] K. E. Riley and P. Hobza, Noncovalent interactions in biochemistry, *WIREs Computational Molecular Science* **1**, 3 (2011), <https://wires.onlinelibrary.wiley.com/doi/pdf/10.1002/wcms.8>.
- [18] G. A. DiLabio and A. O. de-la Roza, Noncovalent interactions in density-functional theory, arXiv preprint arXiv:1405.1771 (2014), available at <https://arxiv.org/abs/1405.1771>.
- [19] L. A. Burns, A. V. Mayagoitia, B. G. Sumpter, and C. D. Sherrill, Density-functional approaches to noncovalent interactions: A comparison of dispersion corrections (DFT-D), exchange-hole dipole moment (XDM) theory, and specialized functionals, *The Journal of Chemical Physics* **134**, 084107 (2011), [https://pubs.aip.org/aip/jcp/article-pdf/doi/10.1063/1.3545971/14904209/084107.1\\_online.pdf](https://pubs.aip.org/aip/jcp/article-pdf/doi/10.1063/1.3545971/14904209/084107.1_online.pdf).

- [20] H. Gao, S. Imamura, A. Kasagi, and E. Yoshida, Distributed implementation of full configuration interaction for one trillion determinants, *Journal of Chemical Theory and Computation* **20**, 1185 (2024), pMID: 38314701, <https://doi.org/10.1021/acs.jctc.3c01190>.
- [21] K. D. Vogiatzis, D. Ma, J. Olsen, L. Gagliardi, and W. A. de Jong, Pushing configuration-interaction to the limit: Towards massively parallel MCSCF calculations, *The Journal of Chemical Physics* **147**, 184111 (2017), [https://pubs.aip.org/aip/jcp/article-pdf/doi/10.1063/1.4989858/13501842/184111.1\\_online.pdf](https://pubs.aip.org/aip/jcp/article-pdf/doi/10.1063/1.4989858/13501842/184111.1_online.pdf).
- [22] A. Menczer, M. van Damme, A. Rask, L. Huntington, J. Hammond, S. S. Xantheas, M. Ganahl, and O. Legeza, Parallel implementation of the density matrix renormalization group method achieving a quarter petaflops performance on a single dgx-h100 gpu node, *Journal of Chemical Theory and Computation* **0**, null (2024), pMID: 39297788, <https://doi.org/10.1021/acs.jctc.4c00903>.
- [23] X. Ren, J. Zou, H. Zhang, W. Li, and S. Li, Block-correlated coupled cluster theory with up to four-pair correlation for accurate static correlation of strongly correlated systems, *The Journal of Physical Chemistry Letters* **15**, 693 (2024), pMID: 38207241, <https://doi.org/10.1021/acs.jpcclett.3c03373>.
- [24] R. Jin, W. Liang, H. Zhang, Y. Song, Z. Luo, H. Ma, Y. Ma, and Z. Jin, Pisci : A scalable framework for heterogeneous parallel calculation of dynamical electron correlation, in *Proceedings of the 53rd International Conference on Parallel Processing*, ICPP '24 (Association for Computing Machinery, New York, NY, USA, 2024) p. 1103–1113.
- [25] D. W. Schwenke, Introducing MPEC: Massively parallel electron correlation, *The Journal of Chemical Physics* **158**, 084801 (2023), <https://pubs.aip.org/aip/jcp/article-pdf/doi/10.1063/5.0135248/18281269/084801.1.5.0135248.pdf>.
- [26] M. G. Delcey, Multipsi: A python-driven mcscf program for photochemistry and spectroscopy simulations on modern hpc environments, *WIREs Computational Molecular Science* **13**, e1675 (2023), <https://wires.onlinelibrary.wiley.com/doi/pdf/10.1002/wcms.1675>.
- [27] H. H. Corzo, A. E. Hillers-Bendtsen, A. Barnes, A. Y. Zamani, F. Pawłowski, J. Olsen, P. Jørgensen, K. V. Mikkelsen, and D. Bykov, Coupled cluster theory on modern heterogeneous supercomputers, *Frontiers in Chemistry* **11**, 10.3389/fchem.2023.1154526 (2023).
- [28] D. Datta and M. S. Gordon, Accelerating coupled-cluster calculations with gpus: An implementation of the density-fitted ccsd(t) approach for heterogeneous computing architectures

- using openmp directives, *Journal of Chemical Theory and Computation* **19**, 7640 (2023), doi: 10.1021/acs.jctc.3c00876.
- [29] H. Zhai and G. K.-L. Chan, Low communication high performance ab initio density matrix renormalization group algorithms, *The Journal of Chemical Physics* **154**, 224116 (2021), [https://pubs.aip.org/aip/jcp/article-pdf/doi/10.1063/5.0050902/14003774/224116\\_1\\_online.pdf](https://pubs.aip.org/aip/jcp/article-pdf/doi/10.1063/5.0050902/14003774/224116_1_online.pdf).
- [30] X. He, B. Walker, V. H. Man, P. Ren, and J. Wang, Recent progress in general force fields of small molecules, *Curr Opin Struct Biol* **72**, 187 (2022).
- [31] P. S. Nerenberg and T. Head-Gordon, New developments in force fields for biomolecular simulations, *Current Opinion in Structural Biology* **49**, 129 (2018).
- [32] J. W. Ponder and D. A. Case, Force fields for protein simulations, *Adv. Protein Chem.* **66**, 27 (2003).
- [33] J. Mackerell, A. D., Empirical force fields for biological macromolecules: overview and issues, *J Comput Chem* **25**, 1584 (2004).
- [34] W. L. Jorgensen, Monte carlo simulations for free energies of hydration: Past to present, *J Chem Phys* **161**, 10.1063/5.0222659 (2024).
- [35] O. T. Unke, S. Chmiela, H. E. Sauceda, M. Gastegger, I. Poltavsky, K. T. Schütt, A. Tkatchenko, and K.-R. Müller, Machine learning force fields, *Chemical Reviews* **121**, 10142 (2021), doi: 10.1021/acs.chemrev.0c01111.
- [36] J. S. Smith, O. Isayev, and A. E. Roitberg, Ani-1: an extensible neural network potential with dft accuracy at force field computational cost, *Chem. Sci.* **8**, 3192 (2017).
- [37] M. Rezaee, S. Ekrami, and S. M. Hashemianzadeh, Comparing ani-2x, ani-1ccx neural networks, force field, and dft methods for predicting conformational potential energy of organic molecules, *Scientific Reports* **14**, 11791 (2024).
- [38] Y. Alexeev, M. Amsler, M. A. Barroca, S. Bassini, T. Battelle, D. Camps, D. Casanova, Y. J. Choi, F. T. Chong, and C. Chung, Quantum-centric supercomputing for materials science: A perspective on challenges and future directions, *Future Generation Computer Systems* **160**, 666 (2024).
- [39] J. Robledo-Moreno, M. Motta, H. Haas, A. Javadi-Abhari, P. Jurcevic, W. Kirby, S. Martiel, K. Sharma, S. Sharma, and T. Shirakawa, Chemistry beyond exact solutions on a quantum-centric supercomputer, arXiv preprint arXiv:2405.05068 (2024), available at

- <https://arxiv.org/abs/2405.05068>.
- [40] K. Kanno, M. Kohda, R. Imai, S. Koh, K. Mitarai, W. Mizukami, and Y. O. Nakagawa, Quantum-selected configuration interaction: Classical diagonalization of hamiltonians in subspaces selected by quantum computers, arXiv preprint arXiv:2302.11320 (2023), available at <https://arxiv.org/abs/2302.11320>.
- [41] A. Kandala, A. Mezzacapo, K. Temme, M. Takita, M. Brink, J. M. Chow, and J. M. Gambetta, Hardware-efficient variational quantum eigensolver for small molecules and quantum magnets, *Nature* **549**, 242 (2017).
- [42] A. Kandala, K. Temme, A. D. Córcoles, A. Mezzacapo, J. M. Chow, and J. M. Gambetta, Error mitigation extends the computational reach of a noisy quantum processor, *Nature* **567**, 491 (2019).
- [43] Google AI Quantum and Collaborators, Hartree-fock on a superconducting qubit quantum computer, *Science* **369**, 1084 (2020).
- [44] Q. Gao, H. Nakamura, T. P. Gujarati, G. O. Jones, J. E. Rice, S. P. Wood, M. Pistoia, J. M. Garcia, and N. Yamamoto, Computational investigations of the lithium superoxide dimer rearrangement on noisy quantum devices, *The Journal of Physical Chemistry A* **125**, 1827 (2021).
- [45] Q. Gao, G. O. Jones, M. Motta, M. Sugawara, H. C. Watanabe, T. Kobayashi, E. Watanabe, Y. Ohnishi, H. Nakamura, and N. Yamamoto, Applications of quantum computing for investigations of electronic transitions in phenylsulfonyl-carbazole tadf emitters, *npj Computational Materials* **7**, 70 (2021).
- [46] S. Gocho, H. Nakamura, S. Kanno, Q. Gao, T. Kobayashi, T. Inagaki, and M. Hatanaka, Excited state calculations using variational quantum eigensolver with spin-restricted ansätze and automatically-adjusted constraints, *npj Computational Materials* **9**, 13 (2023).
- [47] S. Shirai, H. Iwakiri, K. Kanno, T. Horiba, K. Omiya, H. Hirai, and S. Koh, Computational analysis of chemical reactions using a variational quantum eigensolver algorithm without specifying spin multiplicity, *ACS Omega* **8**, 19917 (2023).
- [48] Y. Nam, J.-S. Chen, N. C. Pienti, K. Wright, C. Delaney, D. Maslov, K. R. Brown, S. Allen, J. M. Amini, and J. Apisdorf, Ground-state energy estimation of the water molecule on a trapped-ion quantum computer, *npj Quantum Information* **6**, 33 (2020).

- [49] I. T. Khan, M. Tudorovskaya, J. J. M. Kirsopp, D. Muñoz Ramo, P. Warrier, D. K. Papanastasiou, and R. Singh, Chemically aware unitary coupled cluster with ab initio calculations on an ion trap quantum computer: A refrigerant chemicals' application, *The Journal of Chemical Physics* **158**, 214114 (2023).
- [50] T. E. O'Brien, G. Anselmetti, F. Gkritis, V. E. Elfving, S. Polla, W. J. Huggins, O. Oumarou, K. Kechedzhi, D. Abanin, R. Acharya, *et al.*, Purification-based quantum error mitigation of pair-correlated electron simulations, *Nature Physics* **19**, 1787 (2023).
- [51] L. Zhao, J. Goings, K. Shin, W. Kyoung, J. I. Fuks, J.-K. Kevin Rhee, Y. M. Rhee, K. Wright, J. Nguyen, J. Kim, and S. Johri, Orbital-optimized pair-correlated electron simulations on trapped-ion quantum computers, *npj Quantum Information* **9**, 60 (2023).
- [52] H. R. Grimsley, S. E. Economou, E. Barnes, and N. J. Mayhall, An adaptive variational algorithm for exact molecular simulations on a quantum computer, *Nature Communications* **10**, 3007 (2019).
- [53] G. Christopoulou, C. Di Paola, F. E. Elzinga, A. Jallat, D. M. Ramo, and M. Krompiec, Quantum hardware calculations of the activation and dissociation of nitrogen on iron clusters and surfaces, *Physical Chemistry Chemical Physics* **26**, 5895 (2024).
- [54] A. Eddins, M. Motta, T. Gujarati, S. Bravyi, A. Mezzacapo, C. Hadfield, and S. Sheldon, Doubling the size of quantum simulators by entanglement forging, *PRX Quantum* **3**, 010309 (2022).
- [55] M. Motta, G. O. Jones, J. E. Rice, T. P. Gujarati, R. Sakuma, I. Liepuoniute, J. M. Garcia, and Y.-y. Ohnishi, Quantum chemistry simulation of ground-and excited-state properties of the sulfonium cation on a superconducting quantum processor, *Chemical Science* **14**, 2915 (2023).
- [56] M. A. Castellanos, M. Motta, and J. E. Rice, Quantum computation of  $\pi \rightarrow \pi^*$  and  $n \rightarrow \pi^*$  excited states of aromatic heterocycles, *Molecular Physics* **122**, e2282736 (2024).
- [57] I. Liepuoniute, M. Motta, T. Pellegrini, J. E. Rice, T. P. Gujarati, S. Gil, and G. O. Jones, Simulation of a diels-alder reaction on a quantum computer, arXiv preprint arXiv:2403.08107 (2024), available at <https://arxiv.org/abs/2403.08107>.
- [58] T. Weaving, A. Ralli, P. J. Love, S. Succi, and P. V. Coveney, Contextual subspace variational quantum eigensolver calculation of the dissociation curve of molecular nitrogen on a superconducting quantum computer, arXiv preprint arXiv:2312.04392 (2024), available at

- <https://arxiv.org/abs/2312.04392>.
- [59] J. I. Colless, V. V. Ramasesh, D. Dahlen, M. S. Blok, M. E. Kimchi-Schwartz, J. R. McClean, J. Carter, W. A. de Jong, and I. Siddiqi, Computation of molecular spectra on a quantum processor with an error-resilient algorithm, *Physical Review X* **8**, 011021 (2018).
- [60] E. Dimitrov, G. Sanchez-Sanz, J. Nelson, L. O’Riordan, M. Doyle, S. Courtney, V. Kannan, H. Naseri, A. G. Garcia, J. Tricker, *et al.*, Pushing the limits of quantum computing for simulating pfas chemistry, arXiv preprint arXiv:2311.01242 (2023), available at <https://arxiv.org/abs/2311.01242>.
- [61] S. Guo, J. Sun, H. Qian, M. Gong, Y. Zhang, F. Chen, Y. Ye, Y. Wu, S. Cao, K. Liu, *et al.*, Experimental quantum computational chemistry with optimized unitary coupled cluster ansatz, *Nature Physics* [10.1038/s41567-024-02530-z](https://doi.org/10.1038/s41567-024-02530-z) (2024).
- [62] C. Hempel, C. Maier, J. Romero, J. McClean, T. Monz, H. Shen, P. Jurcevic, B. P. Lanyon, P. Love, R. Babbush, *et al.*, Quantum chemistry calculations on a trapped-ion quantum simulator, *Physical Review X* **8**, 031022 (2018).
- [63] K. Huang, X. Cai, H. Li, Z.-Y. Ge, R. Hou, H. Li, T. Liu, Y. Shi, C. Chen, D. Zheng, *et al.*, Variational quantum computation of molecular linear response properties on a superconducting quantum processor, *The Journal of Physical Chemistry Letters* **13**, 9114 (2022).
- [64] M. A. Jones, H. J. Vallury, and L. C. L. Hollenberg, Ground-state-energy calculation for the water molecule on a superconducting quantum processor, *Physical Review Applied* **21**, 064017 (2024).
- [65] Y. Kawashima, E. Lloyd, M. P. Coons, Y. Nam, S. Matsuura, A. J. Garza, S. Johri, L. Huntington, V. Senicourt, A. O. Maksymov, *et al.*, Optimizing electronic structure simulations on a trapped-ion quantum computer using problem decomposition, *Communications Physics* **4**, 245 (2021).
- [66] J. J. M. Kirsopp, C. Di Paola, D. Z. Manrique, M. Krompiec, G. Greene-Diniz, W. Guba, A. Meyder, D. Wolf, M. Strahm, and D. Muñoz Ramo, Quantum computational quantification of protein–ligand interactions, *International Journal of Quantum Chemistry* **122**, e26975 (2022).
- [67] V. Leyton-Ortega, S. Majumder, and R. C. Pooser, Quantum error mitigation by hidden inverses protocol in superconducting quantum devices, *Quantum Science and Technology* **8**, 014008 (2023).

- [68] Z. Liang, J. Cheng, H. Ren, H. Wang, F. Hua, Z. Song, Y. Ding, F. T. Chong, S. Han, X. Qian, and Y. Shi, Napa: Intermediate-level variational native-pulse ansatz for variational quantum algorithms, *IEEE Transactions on Computer-Aided Design of Integrated Circuits and Systems* **43**, 1834 (2024).
- [69] P. Liu, R. Wang, J.-N. Zhang, Y. Zhang, X. Cai, H. Xu, Z. Li, J. Han, X. Li, G. Xue, *et al.*, Performing  $su(d)$  operations and rudimentary algorithms in a superconducting transmon qudit for  $d=3$  and  $d=4$ , *Physical Review X* **13**, 021028 (2023).
- [70] P. Lolur, M. Skogh, W. Dobrautz, C. Warren, J. Biznárová, A. Osman, G. Tancredi, G. Wendin, J. Bylander, and M. Rahm, Reference-state error mitigation: A strategy for high accuracy quantum computation of chemistry, *Journal of Chemical Theory and Computation* **19**, 783 (2023).
- [71] A. J. McCaskey, Z. P. Parks, J. Jakowski, S. V. Moore, T. D. Morris, T. S. Humble, and R. C. Pooser, Quantum chemistry as a benchmark for near-term quantum computers, *npj Quantum Information* **5**, 99 (2019).
- [72] J. E. Rice, T. P. Gujarati, M. Motta, T. Y. Takeshita, E. Lee, J. A. Latone, and J. M. Garcia, Quantum computation of dominant products in lithium–sulfur batteries, *The Journal of Chemical Physics* **154**, 134115 (2021).
- [73] R. Santagati, J. Wang, A. A. Gentile, S. Paesani, N. Wiebe, J. R. McClean, S. Morley-Short, P. J. Shadbolt, D. Bonneau, J. W. Silverstone, *et al.*, Witnessing eigenstates for quantum simulation of hamiltonian spectra, *Science Advances* **4**, eaap9646 (2018).
- [74] Y. Shen, X. Zhang, S. Zhang, J.-N. Zhang, M.-H. Yung, and K. Kim, Quantum implementation of the unitary coupled cluster for simulating molecular electronic structure, *Physical Review A* **95**, 020501 (2017).
- [75] S. E. Smart and D. A. Mazziotti, Quantum-classical hybrid algorithm using an error-mitigating  $n$ -representability condition to compute the mott metal-insulator transition, *Physical Review A* **100**, 022517 (2019).
- [76] K. Yamamoto, D. Z. Manrique, I. T. Khan, H. Sawada, and D. M. Ramo, Quantum hardware calculations of periodic systems with partition-measurement symmetry verification: Simplified models of hydrogen chain and iron crystals, *Physical Review Research* **4**, 033110 (2022).
- [77] A. Peruzzo, J. McClean, P. Shadbolt, M.-H. Yung, X.-Q. Zhou, P. J. Love, A. Aspuru-Guzik, and J. L. O’Brien, A variational eigenvalue solver on a photonic quantum processor, *Nature*



- communications **5**, 4213 (2014).
- [78] P. J. O'Malley, R. Babbush, I. D. Kivlichan, J. Romero, J. R. McClean, R. Barends, J. Kelly, P. Roushan, A. Tranter, and N. Ding, Scalable quantum simulation of molecular energies, *Physical Review X* **6**, 031007 (2016).
- [79] M. Loipersberger, F. D. Malone, A. R. Welden, R. M. Parrish, T. Fox, M. Degroote, E. Koyseva, N. Moll, R. Santagati, and M. Streif, Accurate non-covalent interaction energies on noisy intermediate-scale quantum computers via second-order symmetry-adapted perturbation theory, *Chemical Science* **14**, 3587 (2023).
- [80] P. J. Ollitrault, M. Loipersberger, R. M. Parrish, A. Erhard, C. Maier, C. Sommer, J. Ullmanis, T. Monz, C. Gogolin, and C. S. Tautermann, Estimation of electrostatic interaction energies on a trapped-ion quantum computer, *ACS Central Science* **10**, 882 (2024).
- [81] B. Jeziorski, R. Moszynski, and K. Szalewicz, Perturbation theory approach to intermolecular potential energy surfaces of van der waals complexes, *Chemical Reviews* **94**, 1887 (1994).
- [82] B. Jeziorski, M. Bulski, and L. Piela, First-order perturbation treatment of the short-range repulsion in a system of many closed-shell atoms or molecules, *International Journal of Quantum Chemistry* **10**, 281 (1976).
- [83] K. Patkowski, Recent developments in symmetry-adapted perturbation theory, *Wiley Interdisciplinary Reviews: Computational Molecular Science* **10**, e1452 (2020).
- [84] L. W. Anderson, M. Kiffner, P. K. Barkoutsos, I. Tavernelli, J. Crain, and D. Jaksch, Coarse-grained intermolecular interactions on quantum processors, *Physical Review A* **105**, 062409 (2022).
- [85] A. A. Holmes, N. M. Tubman, and C. Umrigar, Heat-bath configuration interaction: An efficient selected configuration interaction algorithm inspired by heat-bath sampling, *Journal of Chemical Theory and Computation* **12**, 3674 (2016).
- [86] A. A. Holmes, H. J. Changlani, and C. Umrigar, Efficient heat-bath sampling in fock space, *Journal of Chemical Theory and Computation* **12**, 1561 (2016).
- [87] J. E. Smith, B. Mussard, A. A. Holmes, and S. Sharma, Cheap and near exact cscf with large active spaces, *Journal of Chemical Theory and Computation* **13**, 5468 (2017).
- [88] S. Sharma, A. A. Holmes, G. Jeanmairet, A. Alavi, and C. J. Umrigar, Semistochastic heat-bath configuration interaction method: Selected configuration interaction with semistochastic perturbation theory, *Journal of Chemical Theory and Computation* **13**, 1595 (2017).

- [89] R. J. Bartlett, Perspective on coupled-cluster theory. the evolution toward simplicity in quantum chemistry, *Physical Chemistry Chemical Physics* **26**, 8013 (2024).
- [90] P. Cársky, J. Paldus, and J. Pittner, *Recent progress in coupled cluster methods: Theory and applications*, Challenges and Advances in Computational Chemistry and Physics, Vol. 10 (Springer Science & Business Media, Dordrecht, 2010).
- [91] M. P. Metz, K. Szalewicz, J. Sarka, R. Tóbiás, A. G. Császár, and E. Mátyus, Molecular dimers of methane clathrates: ab initio potential energy surfaces and variational vibrational states, *Physical Chemistry Chemical Physics* **21**, 13504 (2019).
- [92] A. H.-T. Li and S. D. Chao, Interaction energies of dispersion-bound methane dimer from coupled cluster method at complete basis set limit, *Journal of Molecular Structure: THEOCHEM* **897**, 90 (2009).
- [93] E. R. Sayfutyarova, Q. Sun, G. K.-L. Chan, and G. Knizia, Automated construction of molecular active spaces from atomic valence orbitals, *Journal of Chemical Theory and Computation* **13**, 4063 (2017).
- [94] Q. Sun, X. Zhang, S. Banerjee, P. Bao, M. Barbry, N. S. Blunt, N. A. Bogdanov, G. H. Booth, J. Chen, and Z.-H. Cui, Recent developments in the pyscf program package, *The Journal of Chemical Physics* **153**, 024109 (2020).
- [95] Q. Sun, T. C. Berkelbach, N. S. Blunt, G. H. Booth, S. Guo, Z. Li, J. Liu, J. D. McClain, E. R. Sayfutyarova, and S. Sharma, Pyscf: the python-based simulations of chemistry framework, *Wiley Interdisciplinary Reviews: Computational Molecular Science* **8**, e1340 (2018).
- [96] Q. Sun, Libcint: An efficient general integral library for gaussian basis functions, *Journal of Computational Chemistry* **36**, 1664 (2015).
- [97] I. F. Galván, Pegamoid, <https://github.com/Jellby/Pegamoid> (2024), accessed: 2024-09-01.
- [98] F. Neese, Software update: The orca program system - version 5.0, *Wiley Interdisciplinary Reviews: Computational Molecular Science* **12**, e1606 (2022).
- [99] B. Temelso, K. A. Archer, and G. C. Shields, Benchmark structures and binding energies of small water clusters with anharmonicity corrections, *The Journal of Physical Chemistry A* **115**, 12034 (2011).
- [100] J. Rezac and P. Hobza, Describing noncovalent interactions beyond the common approximations: how accurate is the “gold standard,” ccsd(t) at the complete basis set limit?, *Journal*

- of *Chemical Theory and Computation* **9**, 2151 (2013).
- [101] J. Řezáč, P. Jurečka, K. E. Riley, J. Černý, H. Valdes, K. Pluháčková, K. Berka, T. Řezáč, M. Pitoňák, and J. Vondrášek, Quantum chemical benchmark energy and geometry database for molecular clusters and complex molecular systems (www.begdb.com): a user's manual and examples, *Collection of Czechoslovak Chemical Communications* **73**, 1261 (2008).
- [102] M. Motta, K. J. Sung, K. B. Whaley, M. Head-Gordon, and J. Shee, Bridging physical intuition and hardware efficiency for correlated electronic states: the local unitary cluster jastrow ansatz for electronic structure, *Chemical Science* **14**, 11213 (2023).
- [103] P. Jordan and E. P. Wigner, *Über das paulische Äquivalenzverbot* (Springer, 1993).
- [104] G. Aleksandrowicz, T. Alexander, P. K. Barkoutsos, L. Bello, Y. Ben-Haim, D. Bucher, F. J. Cabrera-Hernández, J. Carballo-Franquis, A. Chen, C.-F. Chen, J. M. Chow, A. D. Córcoles-Gonzales, A. J. Cross, A. W. Cross, J. Cruz-Benito, C. Culver, S. D. L. P. González, E. D. L. Torre, D. Ding, E. F. Dumitrescu, I. Duran, P. T. Eendebak, M. Everitt, I. F. Sertage, A. Frisch, A. Fuhrer, J. M. Gambetta, B. G. Gago, J. Gomez-Mosquera, D. Greenberg, I. Hamamura, V. Havlicek, J. Hellmers, Łukasz Herok, H. Horii, S. Hu, T. Imamichi, T. Itoko, A. Javadi-Abhari, N. Kanazawa, A. Karazeev, K. Krsulich, P. Liu, Y. Luh, Y. Maeng, M. Marques, F. Martín-Fernández, D. McClure, D. McKay, S. Meesala, A. Mezzacapo, N. Moll, D. M. Rodríguez, G. Nannicini, P. D. Nation, P. J. Ollitrault, L. J. O'Riordan, H. Paik, J. Pérez, A. Phan, M. Pistoia, V. Prutyaynov, M. Reuter, J. E. Rice, A. R. Davila, R. H. Rudy, M. Ryu, N. Sathaye, C. Schnabel, E. Schoute, K. Setia, Y. Shi, A. Silva, Y. Siraichi, S. Sivarajah, J. A. Smolin, M. Soeken, H. Takahashi, I. Tavernelli, C. Taylor, P. Taylour, K. Trabing, M. Treinish, W. Turner, D. Vogt-Lee, C. Vuillot, J. A. Wildstrom, J. Wilson, E. Winston, C. J. Wood, S. P. Wood, S. Wörner, I. Y. Akhalwaya, and C. Zoufal, *Qiskit: An open-source framework for quantum computing* (2019).
- [105] ffsims developers, ffsim: Faster simulations of fermionic quantum circuits, <https://github.com/qiskit-community/ffsim> (2024), accessed: 2024-09-01.
- [106] A. Javadi-Abhari, M. Treinish, K. Krsulich, C. J. Wood, J. Lishman, J. Gacon, S. Martiel, P. D. Nation, L. S. Bishop, and A. W. Cross, Quantum computing with qiskit, arXiv preprint arXiv:2405.08810 (2024), available at <https://arxiv.org/abs/2405.08810>.
- [107] J. J. Wallman and J. Emerson, Noise tailoring for scalable quantum computation via randomized compiling, *Physical Review A* **94**, 052325 (2016).

- [108] L. Viola and S. Lloyd, Dynamical suppression of decoherence in two-state quantum systems, *Physical Review A* **58**, 2733 (1998).
- [109] A. Kofman and G. Kurizki, Universal dynamical control of quantum mechanical decay: modulation of the coupling to the continuum, *Physical Review Letters* **87**, 270405 (2001).
- [110] M. J. Biercuk, H. Uys, A. P. VanDevender, N. Shiga, W. M. Itano, and J. J. Bollinger, Optimized dynamical decoupling in a model quantum memory, *Nature* **458**, 996 (2009).
- [111] S. Niu and A. Todri-Sanial, Effects of dynamical decoupling and pulse-level optimizations on ibm quantum computers, *IEEE Transactions on Quantum Engineering* **3**, 1 (2022).
- [112] A. A. Saki, S. Barison, B. Fuller, J. R. Garrison, J. R. Glick, C. Johnson, A. Mezzacapo, J. Robledo-Moreno, M. Rossmannek, P. Schweigert, I. Sitdikov, and K. J. Sung, Qiskit addon: sample-based quantum diagonalization, <https://github.com/Qiskit/qiskit-addon-sqd> (2024).
- [113] Y. O. Nakagawa, M. Kamoshita, W. Mizukami, S. Sudo, and Y.-y. Ohnishi, Adapt-qsci: Adaptive construction of input state for quantum-selected configuration interaction, arXiv preprint arXiv:2311.01105 (2023), available at <https://arxiv.org/abs/2311.01105>.
- [114] P. Moritz, R. Nishihara, S. Wang, A. Tumanov, R. Liaw, E. Liang, M. Elibol, Z. Yang, W. Paul, and M. I. Jordan, Ray: A distributed framework for emerging ai applications, arXiv preprint arXiv:1712.05889 (2017), available at <https://arxiv.org/abs/1712.05889>.
- [115] M. Hapka, A. Krzemińska, and K. Pernal, How much dispersion energy is included in the multiconfigurational interaction energy?, *Journal of Chemical Theory and Computation* **16**, 6280 (2020).
- [116] V. von Burg, G. H. Low, T. Häner, D. S. Steiger, M. Reiher, M. Roetteler, and M. Troyer, Quantum computing enhanced computational catalysis, *Physical Review Research* **3**, 033055 (2021).
- [117] N. S. Blunt, J. Camps, O. Crawford, R. Izsák, S. Leontica, A. Mirani, A. E. Moylett, S. A. Scivier, C. Sünderhauf, P. Schopf, J. M. Taylor, and N. Holzmann, Perspective on the current state-of-the-art of quantum computing for drug discovery applications, *Journal of Chemical Theory and Computation* **18**, 7001 (2022), pMID: 36355616, <https://doi.org/10.1021/acs.jctc.2c00574>.
- [118] A. Pyrkov, A. Aliper, D. Bezrukov, Y.-C. Lin, D. Polykovskiy, P. Kanya, F. Ren, and A. Zhavoronkov, Quantum computing for near-term applications in generative chemistry

- and drug discovery, *Drug Discovery Today* **28**, 103675 (2023).
- [119] G. Kumar, S. Yadav, A. Mukherjee, V. Hassija, and M. Guizani, Recent advances in quantum computing for drug discovery and development, *IEEE Access* **12**, 64491 (2024).
- [120] B. Bhushan, P. Pratik, and C. Bhaskar, Chapter 7: The future of drug development with quantum computing, in *High Performance Computing for Drug Discovery and Biomedicine*, edited by A. Heifetz (Springer, 2023) pp. 153–179.
- [121] A. Ralli, M. Williams de la Bastida, and P. V. Coveney, Scalable approach to quantum simulation via projection-based embedding, *Phys. Rev. A* **109**, 022418 (2024).
- [122] H. Lim, D. H. Kang, J. Kim, A. Pellow-Jarman, S. McFarthing, R. Pellow-Jarman, H.-N. Jeon, B. Oh, J.-K. K. Rhee, and K. T. No, Fragment molecular orbital-based variational quantum eigensolver for quantum chemistry in the age of quantum computing, *Scientific Reports* **14**, 2422 (2024).
- [123] T. Yoshikawa, T. Takanashi, and H. Nakai, Quantum algorithm of the divide-and-conquer unitary coupled cluster method with a variational quantum eigensolver, *Journal of Chemical Theory and Computation* **18**, 5360 (2022), pMID: 35926142, <https://doi.org/10.1021/acs.jctc.2c00602>.
- [124] N. Iijima, S. Imamura, M. Morita, S. Takemori, A. Kasagi, Y. Umeda, and E. Yoshida, Towards accurate quantum chemical calculations on noisy quantum computers, *arXiv preprint arXiv:2311.09634* (2023), this preprint is related to the press release of Fujitsu Limited.
- [125] H. Shang, Y. Fan, L. Shen, C. Guo, J. Liu, X. Duan, F. Li, and Z. Li, Towards practical and massively parallel quantum computing emulation for quantum chemistry, *npj Quantum Information* **9**, 33 (2023).

## SUPPLEMENTARY INFORMATION: ACCURATE QUANTUM-CENTRIC SIMULATIONS OF SUPRAMOLECULAR INTERACTIONS

### I. GEOMETRIES OF POTENTIAL ENERGY SURFACES

The PES for the water dimer is calculated for distances between two oxygen atoms ranging between 1.400 and 3.500 Å. We distribute the points for water dimer PES as 1.400, 1.500, 1.600, 1.700, 1.800, 1.900, 1.962, 2.000, 2.100, 2.200, 2.300, 2.400, 2.500, 3.000, and 3.500 Å. All of water dimer simulations are done for all of these distances. The PES for the methane dimer is calculated for the distances between two carbon atoms ranging between 2.500 and 6.000 Å. We distribute the points for methane dimer PES as 2.500, 2.750, 3.000, 3.167, 3.334, 3.500, 3.667, 3.834, 4.000, 4.250, 4.500, 4.750, 5.000, and 6.000 Å. To calculate the total energy of unbound dimer we utilize the distance of 48.000 Å for both water and methane dimers. All of CASCI (16e,16o), CCSD, CCSD(T), CCSD (16e,16o), and CCSD(T) (16e,16o) simulations of methane dimer as well as SQD (16e,16o) simulations with  $|\tilde{\chi}_b| = 20.0 \cdot 10^3$  are done for all of the distances described earlier. The methane dimer CASCI (16e,16o) simulations and SQD (16e,16o) simulations with  $|\tilde{\chi}_b| = 20.0 \cdot 10^3$  are also performed for an additional distance of 3.638 Å. The SQD (16e,16o) energy extrapolations using  $|\tilde{\chi}_b|$  of  $9.0 \cdot 10^3$ ,  $11.0 \cdot 10^3$ , and  $14.0 \cdot 10^3$  are done for 4.000, 4.250, 4.500, 4.750, 5.000, 6.000, and 48.000 Å distances. In the case of HCI (16e,24o) simulations of the methane dimer, we use only distances of 3.638, 3.667, 3.750, 3.834, and 3.900 Å. In case of SQD (16e,24o) simulations we only use the distance of 3.638 Å. All calculations are done as single-point energy calculations with no geometry optimizations. To produce the geometries studies in this work, we start from the equilibrium geometries and change the distance between the centers of the monomers, with the geometries of the individual monomers fixed.

### II. DETAILS OF HCI CALCULATIONS

In HCI simulations instead of generating all of the single and double excitations one generates only those single and double excitations that correspond to Hamiltonian matrix elements exceeding a threshold  $\varepsilon$ . In HCI  $\varepsilon_1$  controls which determinants will be included in the variational wave function. In our HCI calculations, we use values of  $\varepsilon_1$  equal to  $5 \cdot 10^{-6}$  (during initial variational steps) and  $1 \cdot 10^{-6}$  (during later variational steps). We do not

use the non-variational perturbative correction in our HCI calculations. Hence, our HCI calculations are fully variational, which allows for more appropriate comparison between the SQD and HCI results.

### III. EFFECT OF NUMBER OF SAMPLES ON TOTAL ENERGY IN SQD(16E,16O)

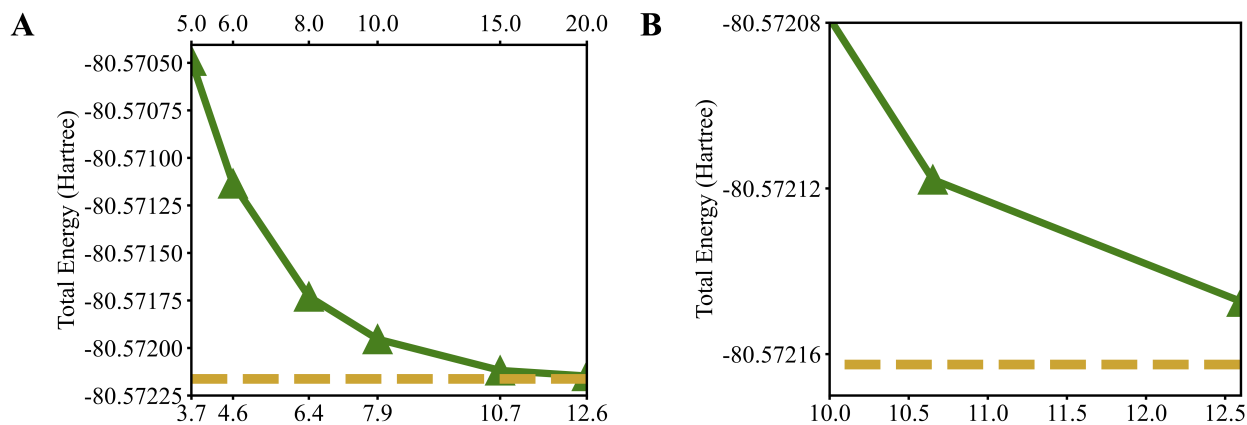


Figure S1. Total energy of methane dimer predicted with SQD (16e,16o) at 3.638  $\text{Å}$  distance between the monomers as the function of  $d \cdot 10^7$ . (A) the entire range of  $d$ , and (B) a magnified region with largest values of  $d$ , highlighted in panel (A) as a black box. The secondary x-axis demonstrates the value of  $|\tilde{\chi}_b| \cdot 10^3$  producing the given value of  $d \cdot 10^7$ . Solid green line with triangular markers shows SQD (16e,16o) results. Horizontal dashed light brown line indicates the total energy from CASCI (16e,16o) calculation.

## IV. PES OF METHANE DIMER INCLUDING THE REPULSIVE REGION

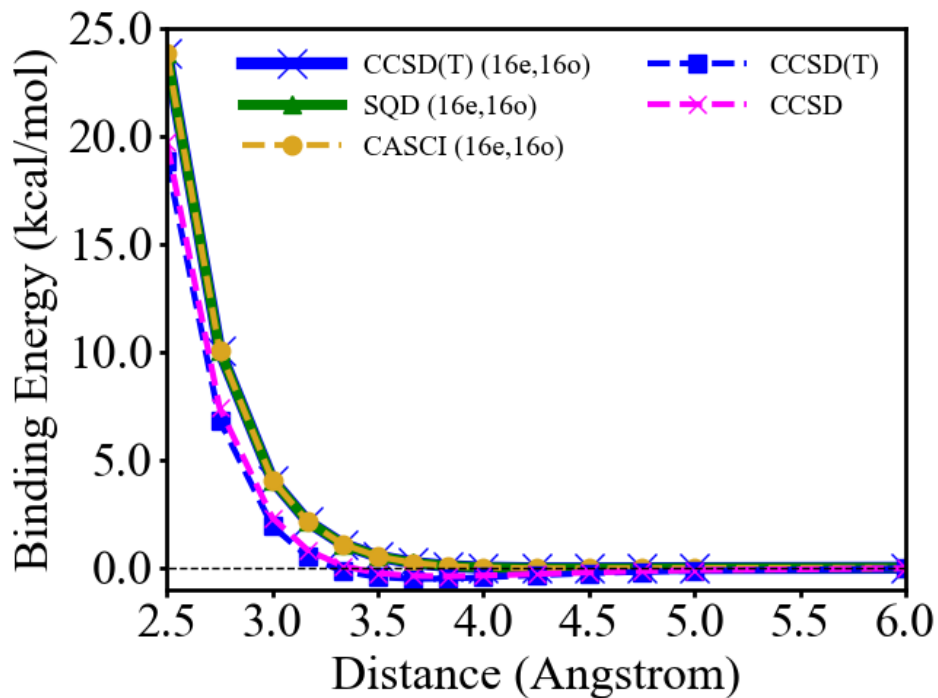


Figure S2. Binding energies of the methane dimer along its PES, where the distances between the centers of methane molecules range between 2.500 and 6.000 Å. Active space simulations are performed with (16e,16o). Light brown, orange, and blue dashed lines with circle markers depict PES calculated with CASCI, CCSD, and CCSD(T) methods, respectively. Solid yellow line with triangular markers depicts the PES calculated with the SQD method. Solid blue line represents CCSD(T) calculations using an active space. Black horizontal dashed line indicates the zero value of the binding energy.